Depth From Distortions

Rahul Swaminathan, Ao Wu, Haoyuan Dong

▶ **To cite this version:**

Rahul Swaminathan, Ao Wu, Haoyuan Dong. Depth From Distortions. The 8th Workshop on Omnidirectional Vision, Camera Networks and Non-classical Cameras - OMNIVIS, Rahul Swaminathan and Vincenzo Caglioti and Antonis Argyros, Oct 2008, Marseille, France. inria-00325383

HAL Id: inria-00325383

https://inria.hal.science/inria-00325383

Submitted on 29 Sep 2008

HAL is a multi-disciplinary open access archive for the deposit and dissemination of scientific research documents, whether they are published or not. The documents may come from teaching and research institutions in France or abroad, or from public or private research centers.

L'archive ouverte pluridisciplinaire **HAL**, est destinée au dépôt et à la diffusion de documents scientifiques de niveau recherche, publiés ou non, émanant des établissements d'enseignement et de recherche français ou étrangers, des laboratoires publics ou privés.

Depth From Distortions

Rahul Swaminathan[1,2] and Ao Wu[2] and Haoyuan Dong[2]

[1] Deutsche Telekom Laboratories,
Ernst-Reuter-Platz 7, 10587 Berlin, Germany
[2] Technische Universität Berlin, Germany
Email: rahul.swaminathan@telekom.de

Abstract. Traditionally, images distortions have been regarded as a flaw that needed to be corrected. Much effort has been focused on "undistortion" methods to remedy this shortcoming. However, we see distortions as encoding crucial information about scene structure.
In this paper we describe how scene depth is encoded in the distortions of images acquired with non-single viewpoint cameras or by mosaic construction. We present our framework to exploit these distortions for 3D euclidean reconstruction of scene features from a single image or view. We present methods specifically designed for features such as straight lines, circles or conics and show how it applies to general planar curves as well. Rigorous experimentation using simulations and synthetic images from catadioptric sensors and mosaics are presented.

1 Introduction

Historically, distortions have been considered as an unwanted artifact. As a result, various attempts have been made to calibrate for and remove these distortions. In contrast, this paper presents a framework to exploit images distortions to estimate 3D depth of the scene. Furthermore, we also use distortion for partial camera calibration.

Distortions in images stem from various factors related to the underlying imaging geometry. We specifically refer to imaging geometry, as this includes not only the optical components such as lenses and mirrors of the camera but also the method of image capture such as mosaicing. A complete taxonomy of distortions, based on imaging geometries, has already been studied [1]. This work specifically studied the class of distortions called *caustic distortions*, present in multi-viewpoint images. While distortions in single viewpoint images depend on the imaging geometry alone and can be removed, caustic distortions depend also on scene depth making it impossible to remove unless scene depth is known [1]. In this paper we focus on depth dependant caustic distortions and methods to exploit them for 3D reconstruction.

1.1 Multi-Viewpoint Imagery and Depth.

As the name suggests, non-single viewpoint cameras do not possess a single viewpoint but rather a locus of viewpoints. These viewpoint loci are usually modeled

using caustics [2, 3]. The simplest way to acquire an MVI is by mosaicing [4]. In this case we can model the viewpoint locus simply as the camera trajectory. Another common source of MVIs are catadioptric systems built using lens based cameras and curved mirrors. In general, any curved mirror and lens based camera yields a non-single viewpoint imaging system (see [5–11]for examples). Only specific combinations of mirror shapes, lenses and positioning lead to a single-viewpoint systems [12].

A consequence of viewpoint loci, is that every pixel observes the scene from a different viewpoint. As a result one cannot compute perspective views from MVIs without also knowing scene depth at every image point in the MVI. Any attempt to compute a "near perspective" view leads to distortions called caustic distortions [1]. These distortions therefore encode scene depth that we exploit for 3D reconstruction.

In our framework, the user identifies contours in the image as corresponding to scene lines, circles, or a general curve of known functional form. This is sufficient to compute the Euclidean structure of the selected contours as well as perform partial camera calibration. Note that, unlike in the case of single-view-metrology [13], we do not require metric information nor the existence of parallel lines nor planes for reconstruction.

While the reconstruction of lines using non-single viewpoint catadioptric systems has been demonstrated in the past [14, 15], the full extent of the problem and its scope to general curves and surfaces has not been fully explored beyond its initial proposal in [16]. In fact, the problem applies to more than just catadioptric cameras. Image mosaics, general multi-viewpoint imaging and the study of monocular moving observer and target based trajectory triangulation and tracking [17, 18] all share the same geometric property that we exploit.

We begin by introducing our framework to reconstruct scene structures form one multi-viewpoint image. We present the general framework for planar curves including conics and then present special cases for circles and lines. In general, any scene curve with known functional form can be reconstructed using our approach. We then provide extensive experimental analysis of our reconstruction approach using catadioptric systems. We study the various factors influencing robust reconstruction including imaging system parameters. Finally we provide ground truth verification of our approach on rendered images.

2 Caustic Distortions and Reconstruction

We now present the general theory of 3D reconstruction from one multi-viewpoint image. As mentioned before, the lack of a single viewpoint in MVIs causes image distortions called caustic distortions [1] that depend not only on the imaging geometry but also on scene depth. It is impossible to estimate depth at every pixel from one MVI for arbitrary scenes. However, most urban scenes are rather structured [13] and contain features including lines and curves providing added constraints that we exploit.

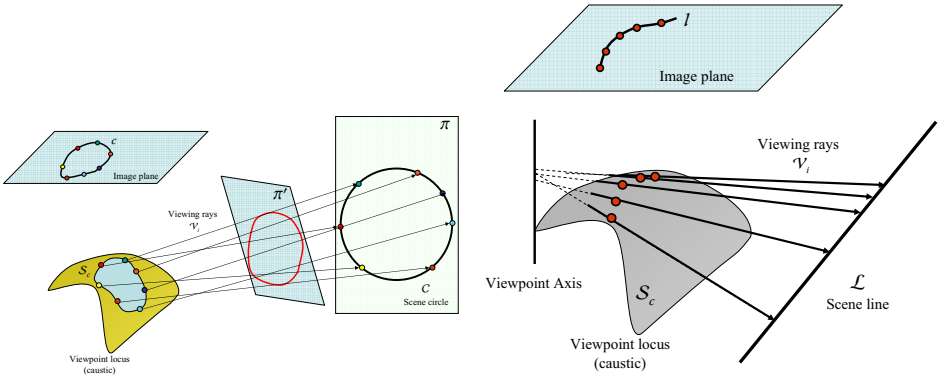

Fig. 1. Distortions in non-single viewpoint images encode scene depth. (a) The skewed viewing rays constrain the shape of the curve formed on the intersection with any plane Π'. Only the real scene plane Π would intersect to form the known scene curve C. (b) An axially non-single viewpoint system imaging a scene line. Proper parameterization of the scene line enables its estimation by solving linear equations in four unknowns.

We begin with the general case of planar curves including conics and then focus on special formulations for circles and lines. However, the method applies directly to non-planar curves and surfaces as well.

2.1 Reconstructing Planar Curves.

Considering the multi-viewpoint image in Fig.1(a), a curve C in the scene on plane Π is imaged as the distorted curve c. We assume the imaging geometry is known for example by calibration [3, 2, 19]. Thus, for any pixel p on c, the viewpoint $\mathbf{S_c}(p)$, and view direction $\mathbf{V_i}(p)$ are known. Conversely, we can define the curve C as the intersection of the viewing rays $\mathbf{V_i}$ with the scene plane Π. Furthermore, any other plane Π' intersecting the ray bundle $\mathbf{V_i}$ results in a curve other than C. Thus, determining C is equivalent to determining Π.[3]

We assume that we know the functional form $\mathcal{F}$ of the curve C, such that for any point P on C, $\mathcal{F}(P) = 0$. This implies we only know the family to which the curve belongs such as a circle, hyperbola, etc and not its exact curve parameters. Reconstruction of C is then posed as a search for the plane parameters $\Pi = [A, B, C, D]$ for which the points of intersection with viewing rays $\mathbf{V_i}$ satisfies the functional form $\mathcal{F}$. The objective function is then:

$$\underset{\{A,B,C,D\}}{\arg\min} \Big(\sum_{N} \big(\mathcal{F}(P)\big) \Big), \tag{1}$$

where P denotes the point of intersection of viewing ray $\mathbf{V_i}(p)$ with plane Π.

[3] It should be noted that this approach works only when the viewing rays $\mathbf{V_i}(p)$ form a set of skewed rays in 3D space. If the rays are coplanar, reconstruction is impossible.

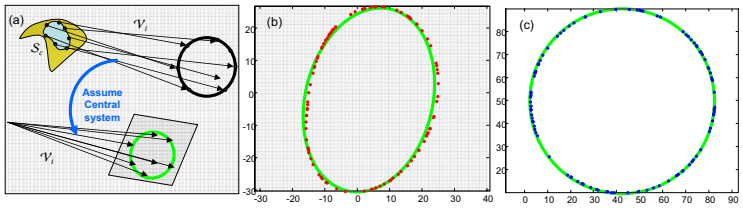

Fig. 2. Reconstructing circles using two steps. (a) Assume the system to be single viewpoint and hallucinate a perspective image. (b) Fit an ellipse to this hallucinated image and thereof determine orientation of the scene circle. (c) Perform full non-linear search using orientation estimate to determine circle in scene.

We apply this approach to conic curves in the experiments to follow. Furthermore, the method directly applies to curves and surfaces in 3D as well.

2.2 Reconstructing Circles.

Robust reconstruction of planar curves, requires a good starting estimate for the four plane parameters $\Pi = [A, B, C, D]$. Circles are special within the space planar curves as they allow for an analytic estimate of three (the plane normal) out of the four parameters, making search faster and more robust.

We first observe that under perspective projection the image of a circle is an ellipse. Also, one can determine the orientation of the circle plane given the elliptic image. We use this property to analytically derive the orientation of the scene plane (3 parameters) to start the non-linear search. Referring to Fig.2(a) we ignore the viewpoint locus and project the rays $\mathbf{V_i}(p)$ from a single point onto a virtual plane to hallucinate a near perspective image of the circle (see Fig.2(b)).[4] We then use the near elliptic image to estimate the orientation of the plane containing the circle (see [20] for details). Using the orientation estimate as a starting point for non-linear search, we optimize for the plane Π that results in a circular intersection with the viewing rays (see Fig.2(c)). This two stage approach performs more robustly and faster than a complete non-linear search.

2.3 Reconstructing Lines.

Lines represent a very special and simple case for reconstruction. It has been shown that: *given four distinct lines in 3D, there exist zero, one, two, or various infinities of lines intersecting the given lines* [21]. In the case of multi-viewpoint images, the skewed viewing rays pass through two lines in theory. One line with positive depth is the scene line and the other, it's geometric complement. In [21], the authors derived a linear solution for the 3D line using a six parameter plücker coordinates. This was later used for catadioptric systems [14, 15].

[4] Note that since the imaging system is non-central, the image produced will not be elliptical. However, this provides a good starting estimate for the non-linear search.

We now present a four parameter linear solution to uniquely estimate the scene line for the case of *axially non-central* imaging systems. By axially non-central we mean that the viewing rays of the multi-viewpoint image pass through a central axis. Most catadioptric systems are axially non-central because they utilize rotationally symmetric mirrors whose axis is aligned with the optical axis of the lens. Fig.1(b), shows such an imaging system where the axis is conveniently chosen to be the $Z-$Axis. Any line L (other than the axis) can be defined as the intersection between plane $\Pi_0 = [A_0\ B_0\ 1\ 0]$, passing through the origin but not parallel to the $Z-$Axis, and plane $\Pi_z = [A_z\ B_z\ 0\ 1]$, parallel to the $Z-$Axis but not passing through the origin.

For a point p on the distorted image l, the viewpoint $\mathbf{S_c}(p) = [0\ 0\ S_c^z]$ on the $Z-$axis, and viewing direction$\mathbf{V_i}(p) = [V_i^x, V_i^y, V_i^z]$ are computed. Now, scene points along these viewing rays can be parameterized as: $P = \mathbf{S_c}(p) + d \cdot \mathbf{V_i}(p)$. The point P lies on the scene line *iff* it lies on both planes Π_0 and Π_z giving:

$$\Big[d \cdot V_i^x, d \cdot V_i^y, S_c^z + d \cdot V_i^z, 1\Big] \cdot \Big[A_0, B_0, 1, 0\Big]' = 0 \tag{2}$$

$$\Big[d \cdot V_i^x, d \cdot V_i^y, S_c^z + d \cdot V_i^z, 1\Big] \cdot \Big[A_z, B_z, 0, 1\Big]' = 0 \tag{3}$$

Now eliminating d from Eqs.(2,3) gives the constraint:

$$\Big[V_i^x, V_i^y, -V_i^x S_c^z, -V_i^y S_c^z\Big] \cdot \Big[A_0, B_0, A_z, B_z\Big]' = -V_i^z \tag{4}$$

Thus, solving for the 3D position of the scene line reduces to a linear problem of estimating the four parameters of the intersecting planes.

3 Reconstruction Using Catadioptric Cameras

We now present exhaustive experimental evaluation and analysis of reconstruction using non-single viewpoint catadioptric cameras. We focus on catadioptric cameras using commonly used quadric (spherical, parabolic or hyperbolic) mirrors. We begin with numerous simulations with noise and study the effect of various imaging and scene parameters on reconstruction. Next, we present a real working experiment with rendered images. A rendered scene is used to compare the quality of reconstruction, using the entire pipeline including the user interaction, against known ground truth.

A complete understanding of how noise affects reconstruction also involves understanding the effects of mirror shape, size as well as the position of the reconstructed structure in the scene. We present these dimensions of error analysis in the subsequent sections.

3.1 Reconstruction of Conics.

We begin with the reconstruction of general conic shaped objects in the scene. These include elliptic, parabolic and hyperbolic curves in the scene. We consider circles and lines subsequently as special cases of conics.

Fig.3(a) shows a typical catadioptric image of a scene containing an ellipse (in blue), parabola(green) and a hyperbola(black), acquired using a perspective lens and a spherical reflector. The images with other quadric mirrors are similar. Under zero noise conditions all catadioptric systems reconstruct the conics perfectly as seen in Fig.3(b). With increase in noise in pixels along the image contour, reconstruction errors predictably increase. We present two sample noise level of 0.5 and 1.0 pixels in Figs.3(c,d).

3.2 Reconstruction of Circles.

Circles as mentioned earlier represent a special case of conics due to their symmetry. We use the two stage method described in Section 2.2 to reconstruct scene circles.

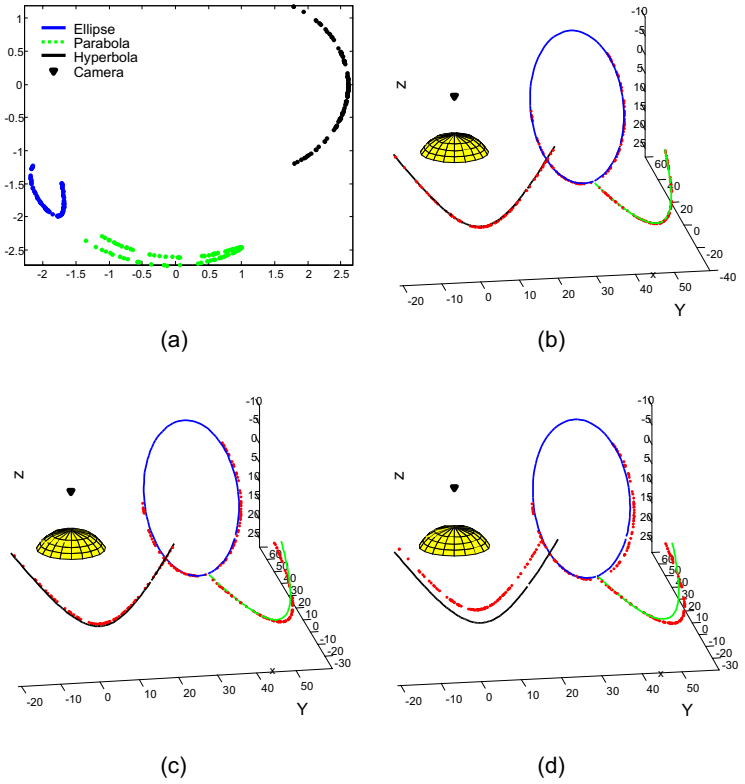

Fig. 3. Reconstruction results of conics in the scene using quadric mirror based non-single viewpoint catadioptric cameras. (a) Catadioptric image using a perspective lens and a spherical mirror shows the distorted image of these scene conics. (b) We harness exploit the depth encoded due to *caustic distortions* to reconstruct the conics in 3D accurately (noiseless case). Reconstruction degrades gracefully with increasing noise as shown under simulations of uniform noise distributions of (c) 0.5 and (d) 1.0 pixels.

Figs.4(a-h) show results of reconstructing multiple circles in the scene using various types of catadioptric imaging systems. In Fig.4(a) the typically distorted image of the circles acquired with a spherical mirror based system is shown. The images due to the other mirror shapes are similar in nature and hence not presented. Under zero noise conditions, every catadioptric systems obviously perform perfect reconstruction as seen in Fig.4(b). Subsequent reconstructions using a spherical (c,d), parabolic (e,f) and hyperbolic (g,h) mirrors with uniform distributions of 0.5 and 1.0 pixels respectively are also presented.

A careful observation shows that the spherical mirror based catadioptric camera outperforms both, the parabolic and hyperbolic mirror based systems. A more complete comparison of these mirror shapes is provided after studying reconstructions of lines.

3.3 Line reconstruction with noise.

We now present results of the simplest form case of reconstructing scene structures that of reconstructing scene lines from a single non-single viewpoint image.

Figs.5(a-h), show the reconstruction of various lines in the scene at different positions using various types of catadioptric cameras. Similar to the results with circle reconstruction, in Fig.5(a) we present a typical distorted image of the scene line in a spherical mirror based system. In Fig.5(b), we present the reconstruction of these lines from the image points under no noise conditions. Again, all mirror based systems reconstruct the lines precisely. Figs.5(c,d),(e,f),(g,h) now present reconstructions of the same scene lines using a spherical, parabolic, and hyperbolic mirror and under two noise conditions (0.5, 1.0 pixels) respectively.

Again, it can be observed that the spherical mirror based systems Figs.5(c,d) outperform both the parabolic and hyperbolic mirror based systems.

3.4 Reconstruction and Mirror Shapes.

In the last two sections we noticed that the spherical mirror seemed to outperform the other mirror shapes in reconstruction. This observation behoved us to verify this hypothesis experimentally.

We chose lines for these experiments as their reconstruction is linear and thus faster to compute. As seen in Fig.6(a), after tens of thousands of simulations of line reconstructions under various noise conditions, it is clear that the spherical mirror based system consistently has lower reconstruction error (black curve), than any other mirror based catadioptric system. The tests were conducted under comparable conditions such as scene structure depth and field of view of the cameras. Moreover, the hyperbolic mirror is actually far worse than any other mirror based system. Another intriguing phenomenon, was the linear relationship between reconstruction error and noise.

3.5 Reconstruction and Mirror Size.

Robustness of reconstruction from non-single viewpoint images depends heavily on the size of the underlying viewpoint locus or caustic. The bigger the mirror,

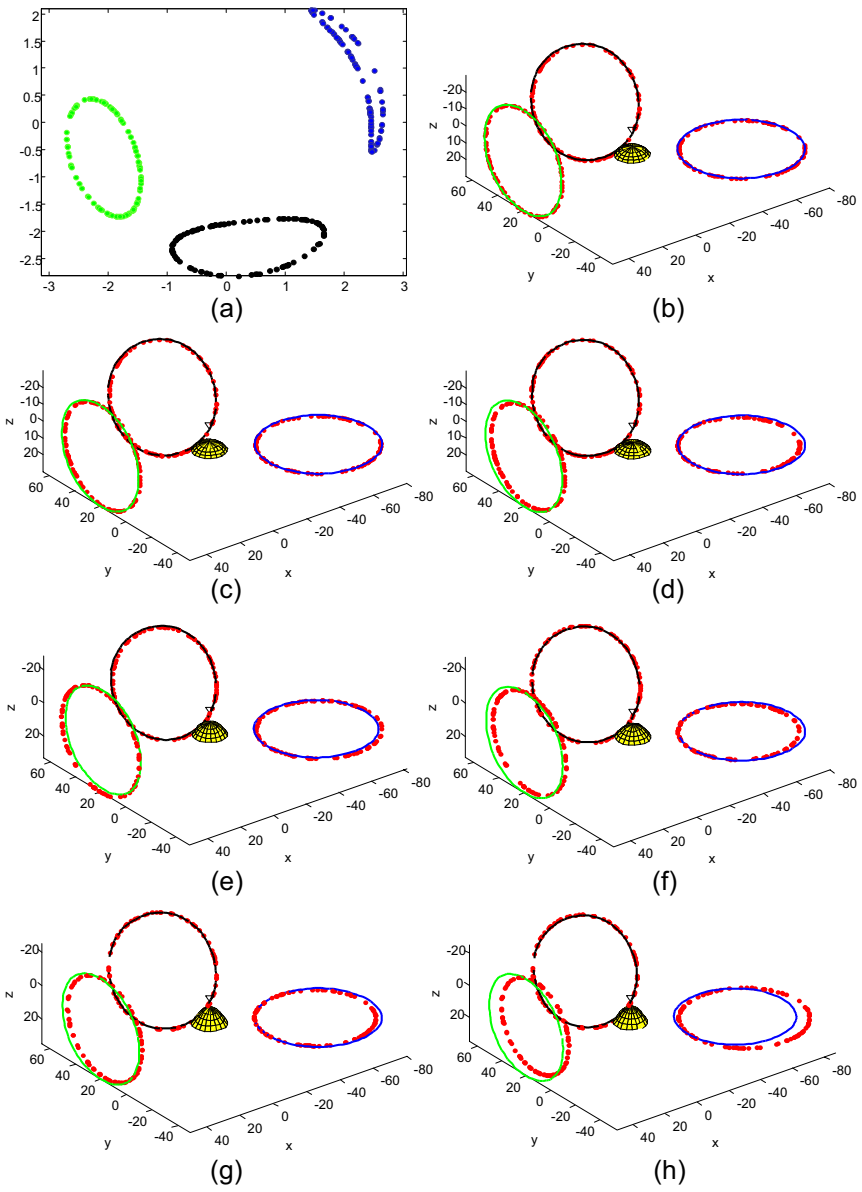

Fig. 4. Reconstruction of circles in the scene. (a) The distorted image of circles in the scene acquired using a perspective lens and a spherical mirror based catadioptric camera. (b) Under noiseless conditions all catadioptric systems produce accurate 3D reconstructions. Reconstructions using a spherical (c,d), parabolic (e,f), and hyperbolic (g,h) mirror degrade gracefully with increasing noise in the uniform interval (0.5,1.0) pixels.

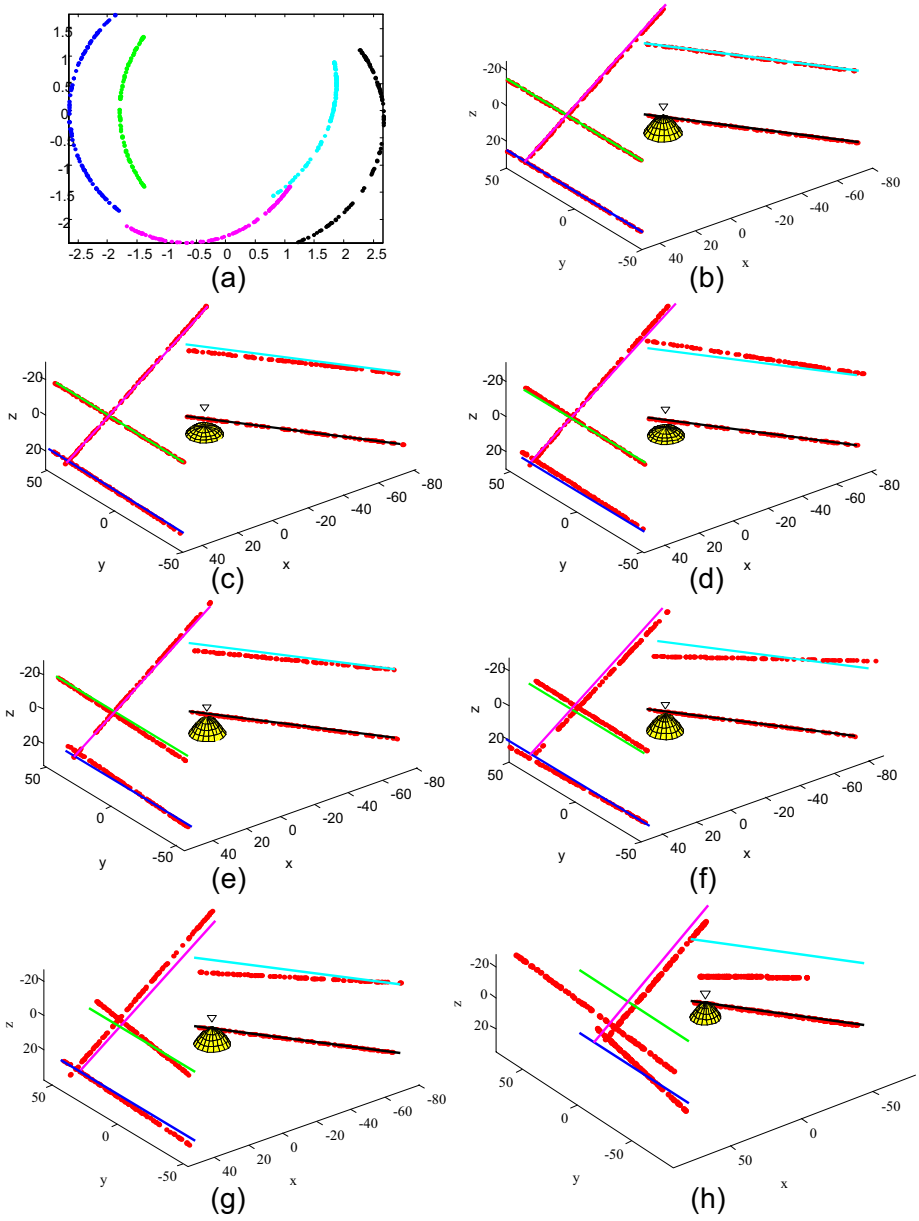

Fig. 5. Reconstruction of scene lines using non-single viewpoint catadioptric cameras. (a) An example of distortions in the images of scene lines acquired using a spherical mirror based system. (b) Under noiseless conditions all catadioptric systems produce accurate 3D reconstructions. Reconstructions using a spherical (c,d), parabolic (e,f), and hyperbolic (g,h) mirror degrade gracefully with increasing noise in the uniform interval (0.5,1.0) pixels. Spherical mirror based system seems to outperform other catadioptric systems.

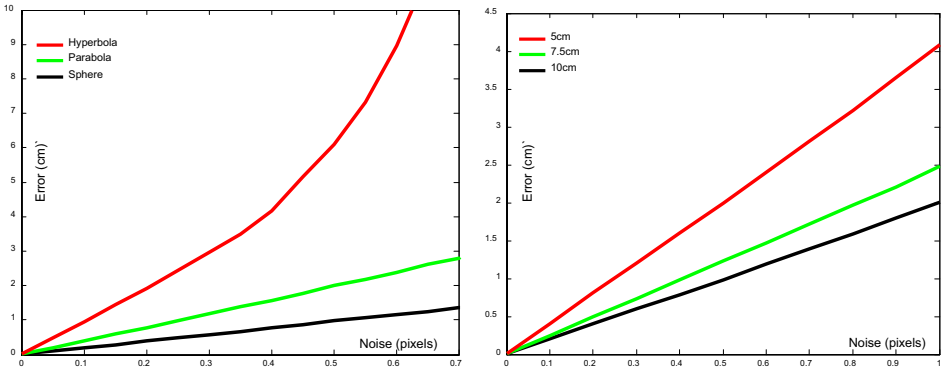

Fig. 6. (a)Comparison of mirror shape and reconstruction error of scene lines. Thousands of simulations at various simulated noise conditions show that the spherical mirror based system (black curve) definitely outperforms both the parabolic (green) and hyperbolic (red) mirror based systems. (b) Comparison of mirror size and reconstruction error of scene lines. The thousands of simulations at various simulated noise conditions for three spherical mirror radii show that mirror size does matter. The largest mirror (black curve) also has the largest viewpoint locus aiding robust reconstruction.

the larger the caustic is likely to be. This means, for a given scene structure, its image would undergo greater caustic distortion. A consequence of this is higher robustness to noise during reconstruction.

We studied this hypothesis for the case of spherical mirror as they were experimentally shown to be the best of the three mirror shapes studied. Fig.6(b) shows a comparison of reconstruction error against mirror radius. Note that the mirror was appropriately located below the entrance pupil at increasing distances so as to ensure the system had the same effective field of view. As can be seen from the plots, the larger the radius, the better the reconstruction.

3.6 Reconstruction and Target Position.

The above analysis of mirror shape and size assumed arbitrary scene structure (line) positions. The error presented was the average across multiple line positions and orientations. However, the position of the scene structure is also critical to robust reconstruction. This again has close relationship to the underlying caustic or viewpoint locus surface's shape and size.

Referring to Fig.7(a), we consider a spherical mirror and its associated caustic or viewpoint locus. Considering the vertical cross sectional plane, we consider scene lines equidistant from the spherical mirror centre orthogonal to this plane. We know from theory that any structure corresponding to the plane passing through the *axis* or the *horizon* (shown in red) cannot be reconstructed because the viewing rays are coplanar. Thus close to these ray direction, reconstruction errors should be large. For other viewing direction along the mirror the errors should be minimal.

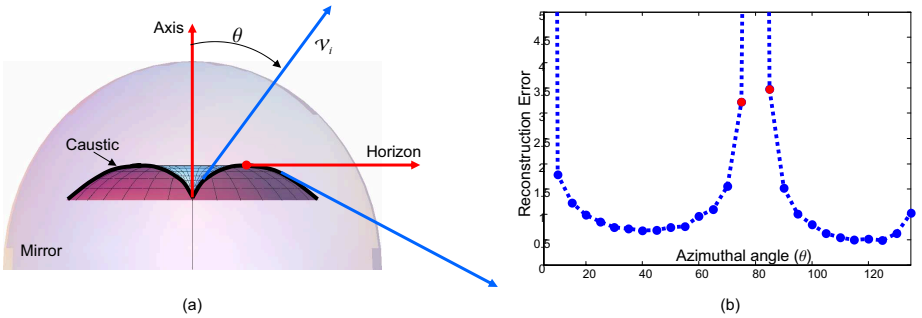

Fig. 7. Experimental study of line position and reconstruction errors. (a) Setup showing the axis and the horizon rays where the viewing rays are coplanar making reconstruction impossible. Scene lines were synthesized and tested for reconstruction errors across the vertical field of view. (b) Errors are as expected high at these singular points and become lower elsewhere.

Results from our experiment (see Fig.7(b)) in fact verify our prediction. Errors starting at $\theta = 0$ along the axis are high and then decrease initially before rising again towards the horizon. Beyond the horizon, reconstruction errors decrease once again only to increase towards end of the field of view. Moreover, reconstruction error below the horizon (where the caustic is large and spread out) seems to be lower than in the section between the apex and the horizon where the caustic is compact).

The effect of mirror shape, size and location in fact are all closely tied to the local caustic size and extent. Analogous to stereo baseline, the larger the caustic the better the reconstruction (see [20, 22] for details).

3.7 Experiment on Rendered Image.

We finally present experimental results on rendered images of typical urban interiors. We use rendered images because while we still have *ground truth*, we can still test the entire pipeline used for reconstruction including the user interaction and automatic gradient based contour detection. The details of the user interface and tools for semi-automatic detection of edge contours in the distorted image is beyond the scope of this paper (see [22] for details). We present results under two scenarios: (1) a non-central catadioptric imaging system and (2) a centre strip mosaic.

Fig.8 (a) shows a catadioptric image acquired with a spherical mirror of radius 7.5cm and a perspective lens based camera rendered using PovRay. The room is roughly 5×5m in size. We assume the catadioptric system is calibrated. Using our semi-automatic tool, edge contours in the image are identified as being lines, or circles respectively as in Fig.8 (b). We then reconstruct the various scene structures using the proposed methods. The reconstructed features (shown in red) are then rendered in the original scene for visualization from two perspectives as seen in Fig.8 (c,d).

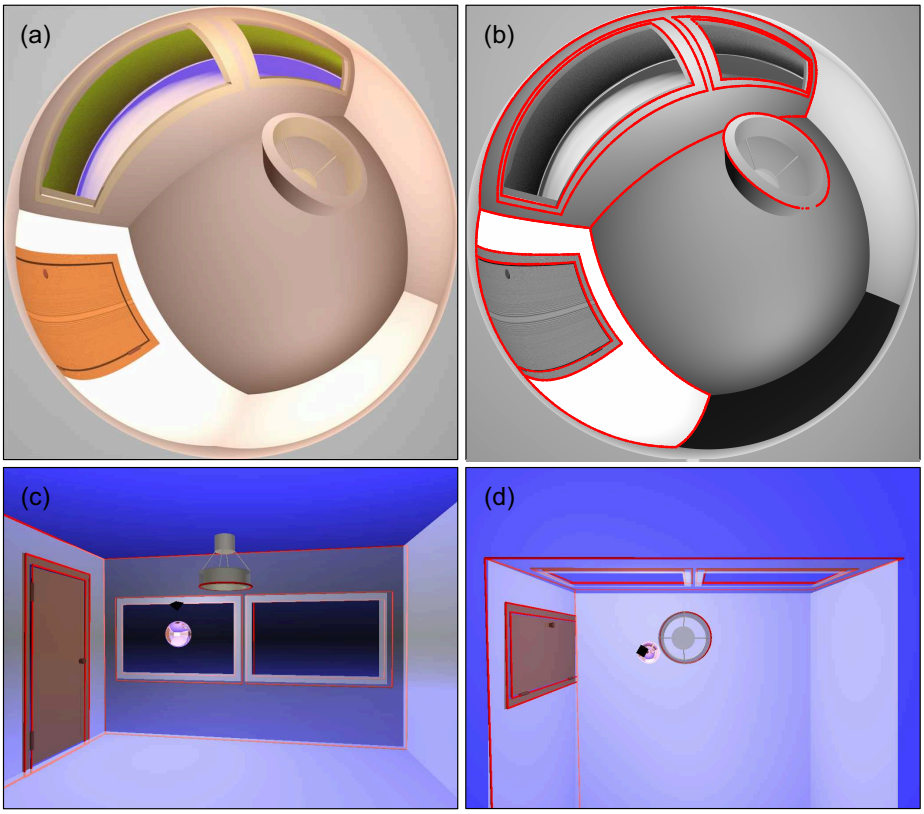

Fig. 8. Reconstruction of a rendered scene using the *depth from distortions* framework. (a) The original catadioptric image of a room 5×5m in size. (b) Points along contours in the image are semi-automatically extracted and reconstructed. (c,d) With the knowledge of which contour is a line or circle in the scene, we perform Euclidean reconstruction of these structures using the proposed methods. The reconstructed structures (in red) are superimposed on the ground truth views of the scene.

Fig.9 (a) shows a centre-strip mosaic computed by rotating a camera off axis along a known circular trajectory. Again the user identifies edges in the mosaic using the semi-automatic tool as belonging to scene features such as lines or circles respectively. Figs.9 (b,c) show the reconstructed features (solid red and blue lines) in the room using the proposed methods. We show two views to avoid perspective ambiguities in visualizing the reconstruction.

As seen in both cases of the catadioptric imaging system as well as the mosaic, accurate reconstruction is possible from a single multi-viewpoint image given identifiable structures in the scene.

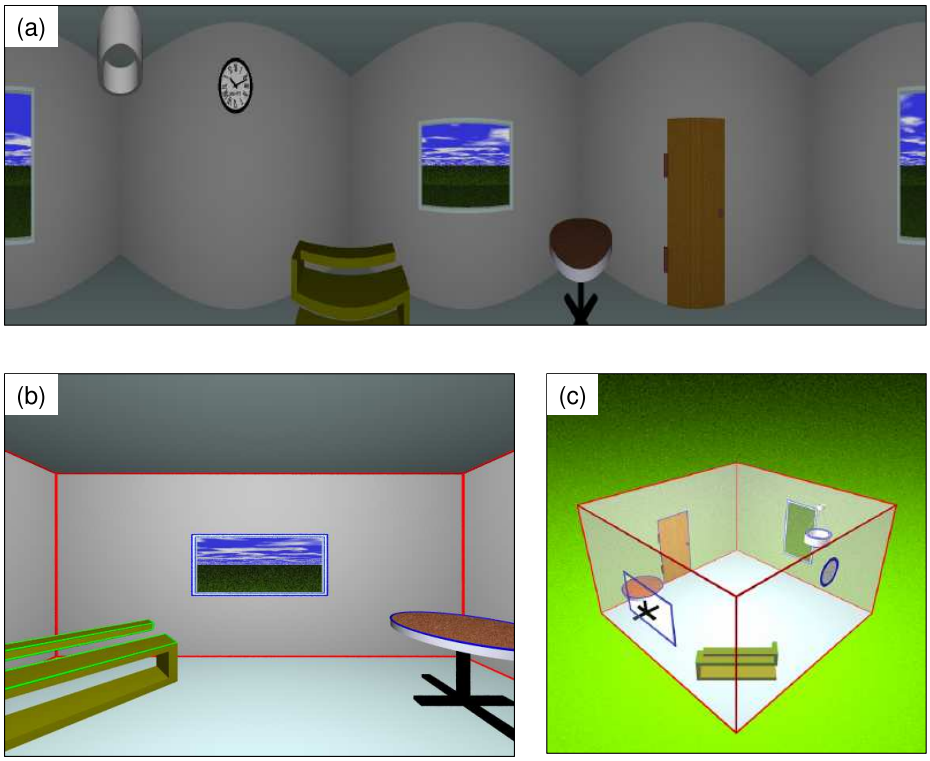

Fig. 9. Reconstruction of a room from a single centre-strip mosaic. (a) The original mosaic image computed by collating the centre column of pixels of an off-axis rotating camera. Marked edge contours semi-automatically detected are then reconstructed. (b,c) Two views from within and outside the room of the reconstructed features overlaid (solid lines) on the ground truth scene structure.

4 Conclusion

In this paper we presented a general framework for 3D reconstruction from a single image acquired either as mosaics or using non-single viewpoint cameras. In general any curve in the scene of known functional form can be reconstructed in this manner. We presented a detailed noise analysis by reconstructing numerous scene curves and lines using various catadioptric systems. We also analyzed the factors affecting reconstruction quality such as imaging system design and the scene itself. We find that reconstruction robustness depends on various aspects that effectively measure the size of the underlying *caustic* or viewpoint locus. In some sense this is similar to the baseline in stereo.

Reconstruction of rendered scenes simulating a catadioptric sensor and mosaic image was performed for comparison with ground truth. While distortions have been historically regarded as an unwanted artifact, we showed how they can be exploited to our advantage for reconstruction.

References

1. Swaminathan, R., Grossberg, M.D., Nayar, S.K.: A Perspective on Distortions. In: Proc. CVPR. (2003) II: 594–601
2. Swaminathan, R., Grossberg, M.D., Nayar, S.K.: Non-Single Viewpoint Catadioptric Cameras: Geometry and Analysis. IJCV **66** (2006) 211–229
3. Grossberg, M.D., Nayar, S.K.: The Raxel Imaging Model and Ray-Based Calibration. IJCV **61** (2005) 119–137
4. Peleg, S., Rousso, B., Rav-Acha, A., Zomet, A.: Mosaicing on adaptive manifolds. PAMI **22** (2000) 1144–1154
5. Yagi, Y., Yachida, M.: Real-Time Generation of Environmental Map and Obstacle Avoidance Using Omnidirectional Image Sensor with Conic Mirror. In: Proc. CVPR. (1991) 160–165
6. Bogner, S.: Introduction to Panoramic Imaging. In: IEEE SMC Conference. Volume 54. (1995) 3100–3106
7. Chahl, J., Srinivasan, M.: Reflective Surfaces for Panoramic Imaging. Applied Optics **36** (1997) 8275–8285
8. Bruckstein, A., Richardson, T.: Omniview Cameras with Curved Surface Mirrors. In: Proc. OMNIVIS. (2000) 79–84
9. Svoboda, T., Pajdla, T., Hlaváč, V.: Central Panoramic Cameras: Design and Geometry. In: Proc. of Computer Vision Winter Workshop in Slovenia. (1998) 120–133
10. Gächter, S.: Mirror Design for an Omnidirectinal Camera with a Uniform Cylindrical Projection when using the SVAVISCA Sensor. Technical Report CTU-CMP-2001-03, Czech Technical University (2001)
11. Hicks, R., Perline, R.: Geometric Distributions for Catadioptric Sensor Design. In: Proc. CVPR. (2001) I:584–589
12. Baker, S., Nayar, S.K.: A Theory of Catadioptric Image Formation. In: Proc. ICCV. (1998) 35–42
13. Criminisi, A., Reid, I., Zisserman, A.: Single View Metrology. International Journal of Computer Vision **40** (2000) 123–148
14. Caglioti, V., Gasparini, S.: On the Localization of Straight Lines in 3D Space from Single 2D Images. In: Proc. CVPR. (2005) I:1129–1134
15. Lanman, D., Wachs, M., Taubin, G., Cukierman, F.: Reconstructing a 3D Line from a Single Catadioptric Image. In: 3DPVT'06: Proc. Third Intl Symposium on 3D Data Processing, Visualization, and Transmission. (2006) 89–96
16. Swaminathan, R.: Non-Perspective Imaging Systems. PhD thesis, Columbia University, New York, NY, USA (2003)
17. Naeve, A.: Structure from Translational Observer Motion. In: Proc. of the Intl. Workshop on Algebraic Frames for the Perception-Action Cycle. (1997) 235–248
18. Avidan, S., Shashua, A.: Trajectory triangulation: 3d reconstruction of moving points from a monocular image sequen. PAMI **22** (2000) 348–357
19. Sturm, P., Ramalingam, S.: A generic concept for camera calibration. In: OMNIVIS. (2004) Vol II: 1–13
20. Wu, A.: 3D Reconstruction from a Single Image. Diplomarbeit in fachgebiet nachrichtenuebertragung, Technische Universität Berlin, Germany (2008)
21. Teller, S., Hohmeyer, M.: Determining the lines through four lines. Journal of Graph. Tools **4** (1999) 11–22
22. Swaminathan, R., Wu, A., Dong, H.: Depth cues in multi-viewpoint imaging. Technical Report 4, Deutsche Telekom Laboratories (2008)